# Polarized Absorption and Reflection Spectra of the Single Crystals of Benzidine–7,7,8,8-Tetracyano-*p*-quinodimethane Molecular Complexes

Kyuya YAKUSHI, Masaaki IGUCHI, and Haruo KURODA*

*Department of Chemistry, Faculty of Science, The University of Tokyo, Hongo, Tokyo 113*

(Received March 9, 1979)

Polarized absorption and reflection spectra were observed on the single crystals of the solvent-free and solvent-containing modifications of benzidine (BD)–7,7,8,8-tetracyano-*p*-quinodimethane (TCNQ) molecular complex, by using the microspectrophotometers of transmission and reflection types. The absorption spectra obtained by the dispersion analyses of the reflection spectra agreed fairly well with those directly observed by the transmission method. The spectra showed that the BD–TCNQ complex has non-ionic ground state in all modifications although the intermolecular interaction is considerably strong and is appreciably affected by the inclusion of solvent molecules. In all modifications, the second charge-transfer band was confirmed to be polarized in the direction almost perpendicular to the direction of the donor-acceptor stack, while the first charge transfer band is polarized in the direction of the donor-acceptor stack as it is usually found for a typical charge-transfer complex. This anomaly of the polarization direction of the second charge-transfer band was concluded to be due to a strong mixing between the charge-transfer excitation and the local excitation associated with TCNQ.

The charge-transfer complex which involves benzidine (BD) as electron donor and 7,7,8,8-tetracyano-*p*-quinodimethane (TCNQ) as electron acceptor, exhibits anomalous behaviors in several respects. First, BD–TCNQ is not a radical salt, but a charge-transfer complex with essentially non-ionic ground state, although BD is an electron donor with considerably low ionization potential (7.0 eV) and TCNQ is an electron acceptor with very high electron affinity (2.8 eV).[1] Second, when BD–TCNQ complex is crystallized from solution, it forms either a crystal including solvent molecules in the crystal lattice or a crystal of the solvent-free form, depending on the solvent used, and the semiconductive properties of the solvated modifications are markedly different from those of the solvent-free modification.[2,6] The crystal structure analyses revealed that, in the solvated modifications, solvent molecules are included in the channel-like free space in the BD–TCNQ host-lattice, while BD and TCNQ molecules are closely packed without leaving any space to accommodate solvent molecules in the case of the solvent-free modification.[3–5] From these structural studies, the solvated modifications of BD–TCNQ complex were concluded to be a new type of the inclusion compound where the intermolecular hydrogen bonds and intermolecular charge-transfer interaction are responsible for the formation of the channeled structure of the host lattice. The third point of interest is that, according to our preliminary study on the absorption spectrum of BD–TCNQ crystal,[1] the polarization direction of the second charge-transfer band is perpendicular to the direction of the BD–TCNQ stack while the first charge transfer band is parallel to the stacking direction as it is usually expected for a typical charge-transfer band.

In view of those anomalous behaviors of BD–TCNQ system, it seemed of great interest to investigate the optical properties of the single crystals of the solvent-free and solvated modifications of BD–TCNQ complex.

As we have pointed out in our previous papers,[3–5] the obtainable modifications of BD–TCNQ complex can be classified into three types according to the difference as regards the structure of the BD–TCNQ sub-lattice: the one is the solvent free modification, the second is the modification which includes an aliphatic solvent molecule such as dichloromethane and the third is the one which includes benzene or its derivatives. Thus, in the present study, we have taken up one representative example for each of these three types: the solvent-free crystal (BD–TCNQ–[n]), the dichloromethane-containing crystal (BD–TCNQ–[$CH_2Cl_2$]), and the benzene-containing crystal (BD–TCNQ–[$C_6H_6$]). We will show the absorption and reflection spectra of these crystals measured by means of the microspectrophotometric technique. Discussion will be given on the interpretation of the observed spectra and on the charge-transfer interaction between BD and TCNQ molecules, using the results of the molecular orbital calculations on the models of isolated BD–TCNQ molecular pair.

## Experimental

*Materials.* The crystals of the solvent-free modification of BD–TCNQ complex were obtained by crystallizing the complex from chloroform solution. The crystals of each solvated modification were prepared from the solution where appropriate amounts of BD and TCNQ were dissolved in the solvent which was to be included in the crystal. The details of the procedure of preparation and the characterization of each modification were described in our previous paper.[6]

*Absorption Spectrum.* The absorption spectrum was measured on very small single crystals by use of plane-polarized light, using the Olympus MSP-A-IV microspectrophotometer which we had modified for the purpose of the measurement of crystal spectrum. The details of this apparatus and the procedure of measurement have been described elsewhere.[7] All absorption spectra were observed at room temperature.

*Reflection Spectrum and Its Analysis.* We have newly constructed an apparatus for the measurement of the reflection spectrum of a very small single crystal. Figure 1 shows the block diagram of this apparatus. We used Sylvania 650 W halogen lamp as the light source for infrared and visible region. The light is monochromatized by means of JASCO-CT52 grating monochromator with the focal length of 50 cm and the *f*-number of 4.5. The monochromatic light is put into the microscope optical system, Olympus

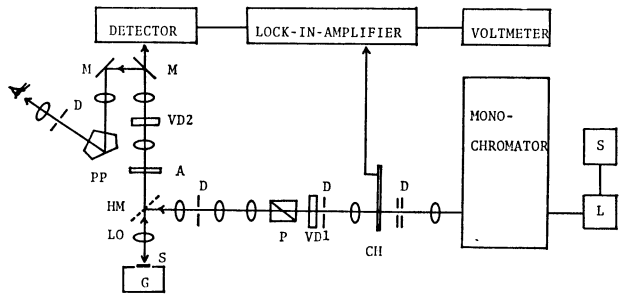


Fig. 1. The optical system of the Olympus MMSP-RK and the block diagram of the microspectrophotometer for reflection spectra. S: A.c. stabilizer, L: 650 W halogen lamp, D: diaphragm, CH: chopper, VD: variable diaphragm, P: polarizer, HM: half mirror, M: mirror, A: analyzer, PP: pentaprism, S: sample, G: goniometer head.

MMSP-RK, the structure of which is schematically illustrated in Fig. 1. In this optical system, the light which has passed through a variable diaphragm (VD1), is converted to a plane-polarized light by a Glan-Thompson prism (P), reflected by a half-mirror (HM), and focussed down onto the sample crystal through an objective lens (LO). The size of the light spot on the sample can be varied from 10 $\mu m\phi$ to 196 $\mu m\phi$ by changing the opening of the variable diaphragm (VD1) and the magnification of the objective lens. The reflected light passes again through the same objective lens, is focussed at the second variable diaphragm (VD2), and the intensity of the light passes through the above diaphragm is measured by the detector. Three detectors, having different spectral sensitivities, are installed and selectively used depending on the wavelength by changing the optical path by means of a mirror system: A photomultiplier tube HTV R435 is used for 400—700 nm region, another tube HTV R316 for 700—1100 nm region and a PbS photoconductive cell, cooled with Dry Ice–methanol mixture, for 1100—2500 nm region.

The output signal from the detector is amplified by a lock-in-amplifier, Brookdeal M9503, by being synchronized to the signals from the remote sensor which detects the rotation of the light chopper (CH), and the final output is read with a digital voltmeter.

The sample crystal is mounted on a goniometer head so that we can select out the crystal face on which the measurement of reflection spectrum is carried out, and can orient the observing crystal face exactly normal to the light axis. The goniometer head is transferable to X-ray diffraction camera to examine the crystallographic character of the observing crystal face. The goniometer head mentioned above is mounted on a rotatable sample stage which also has a mechanism to move in two horizontal directions.

Strictly speaking, the condition of normal incidence is not filled in our optical system, since the light is focussed down onto the sample through the objective lens. The reflectance we are observing, is the one averaged over the contributions of the *s*- and *p*-polarized components of the light beams with the incident directions within the cone of the focusing light. Naturally, the deviation from the normal incidence condition will be larger as the aperture angle of the objective lens is larger. The aperture angles of our lenses are 5.8°, 14.5°, and 23.6° for the magnifications of ×5, ×10, and ×20, respectively. We carried out numerical calculation by computer on the variation of reflectance with incident angle for *s*- and *p*- polarizations.[8] This calculation showed that, when the deviation from the normal incidence direction is less than 24°, the average of the reflectances of the *s*- and *p*-components remains at almost the same value, because the reflectance increases for the *s*-polarization while decreases for the *p*-polarization on increasing the deviation from the normal direction. In effect, the reflectance data which were obtained on the same sample by using the three lenses mentioned above, agreed with each other within the experimental error. Thus we concluded that the reflectance data which are obtainable with our microspectrophotometer can be regarded to be effectively the same as those obtained under the normal incidence condition.

To obtain absolute reflectance values, we have to compare the intensity of the light reflected from the sample with that reflected from a standard reflector of known reflectivity. The single crystals of silicon[9] and saphire[10,11] were used as the standard reflector, since the reflectances of their polished surfaces, in the near-infrared and visible region, are of the same order of magnitude with those of our samples and their surfaces are very stable so that their reflectance values do not vary with time.

On each modification of BD–TCNQ complex, we carried out the measurement on several different crystals. Although the obtained spectral shape were almost the same, the absolute reflectance values were different at most 10% ($\Delta R/R<0.1$) from crystal to crystal depending on the quality of the crystal surface. We considered that the spectrum showing the highest reflectance value at each reflectance maximum, are the best observed result.

There are several different method to obtain optical constants from a reflection spectrum. The Kramers-Kronig analysis is the most direct way if one can use reflectance data over a wide wavelength region. However, in the present study, the observation was limited only in the near-infrared and visible region, and, furthermore, our samples had strong absorption bands around the long and short wavelength limits of the observed range. These situations make it difficult to perform a direct Kramers-Kronig analysis. The method proposed by Roessler[12] and its modification[13] are also hard to be used in the present case. Therefore, we used the so-called dispersion analysis method, describing the complex dielectric function $\varepsilon(\omega)$ by the following equation based on the model of uncoupled Helmholtz-Kettler oscillators:[8]

$$\varepsilon(\omega) = \varepsilon_c + \sum_{j=1}^{N} \frac{S_j\omega_j^2}{(\omega_j^2-\omega^2)-i\gamma_j\omega_j\omega} \tag{1}$$

There is the following relation between the reflectance $R(\omega)$ and the complex dielectric function $\varepsilon(\omega)$.

$$R(\omega) = \frac{|\varepsilon(\omega)|+1-\sqrt{2}\{|\varepsilon(\omega)|+\mathrm{Re}[\varepsilon(\omega)]\}^{1/2}}{|\varepsilon(\omega)|+1+\sqrt{2}\{|\varepsilon(\omega)|+\mathrm{Re}[\varepsilon(\omega)]\}^{1/2}} \tag{2}$$

Treating the constants $\varepsilon_c$ and ($\omega_j$, $\gamma_j$, $S_j$), as adjustable parameters, we determined their values so as to give the best agreement between the observed and calculated reflectance. In this curve-fitting procedure, we defined an error function as $\sum_k[R_{obsd}(\omega_k)-R_{calcd}(\omega_k)]^2$, and looked for the set of the parameter values which minimize the above error function, by means of the Fletcher-Powell method,[14] using computer. By use of the known relations, $\mathrm{Re}[\varepsilon(\omega)]=n(\omega)^2-k(\omega)^2$ and $\mathrm{Im}[\varepsilon(\omega)]=2n(\omega)k(\omega)$, we calculated the optical constants, $n(\omega)$ and $k(\omega)$, from the obtained complex dielectric function. Then, the molar extinction coefficient $\mu(\omega)$ was calculated by Eq. 3

$$\mu(\omega) = \frac{2\omega k(\omega)}{c}\cdot\frac{1000d}{M}, \tag{3}$$

where $c$ is the light velocity in vacuum, $d$ is the density of

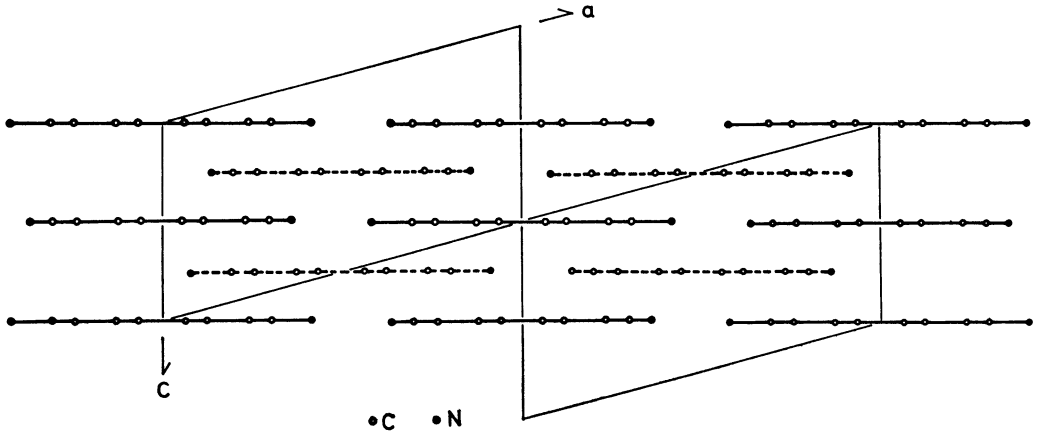


Fig. 2. The crystal structure of BD–TCNQ–[n] projected onto the (010) plane.

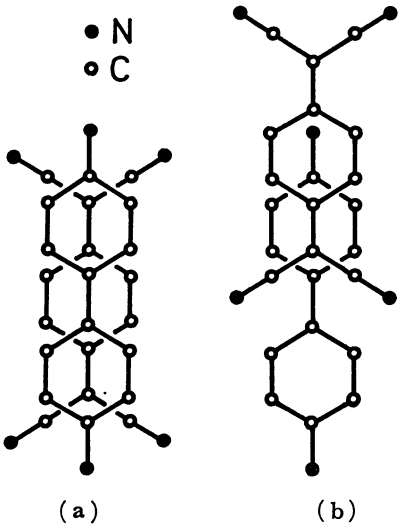


Fig. 3. (a) Molecular overlap between BD and TCNQ (Type A). (b) Molecular overlap between BD and TCNQ (Type B).

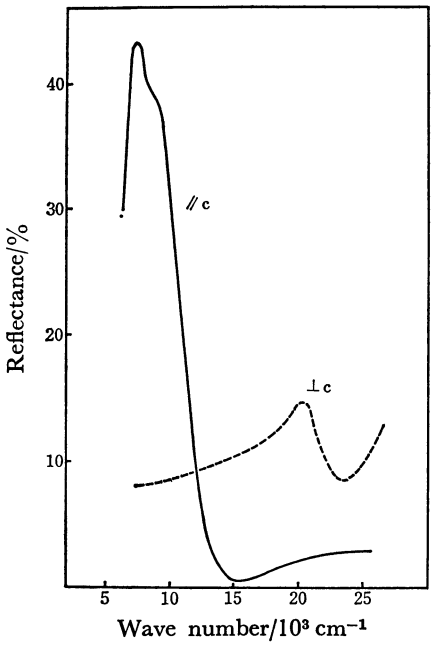


Fig. 4. Reflection spectra on the (010) plane of BD–TCNQ–[n].

the crystal, and $M$ is the molecular weight of the complex. In practice, we used one oscillator function for each transition in describing the complex dielectric function by Eq. 1. The oscillator strength of the $j$-th electronic transition was calculated by the following equation.

$$f(j) = \frac{m}{2\pi^2 e^2 n} \int_0^\infty \mathrm{Im}\varepsilon^{(j)}(\omega)\omega d\omega \qquad (4)$$

where $\varepsilon^{(j)}(\omega) = S_j\omega_j^2/[(\omega_j^2-\omega^2)-i\gamma\omega_j\omega]$, $n$ is the number density of electrons concerned with the $j$-th transition, $m$ is the electron mass, and $e$ is the electron charge.

## Results and Discussion

*Solvent-free Modification, BD–TCNQ–[n].* The crystal of BD–TCNQ–[n] is monoclinic with the space group C2/m. The lattice constants are $a=12.231$ Å, $b=12.679$ Å, $c=6.477$ Å, and $\beta=104.84°$. Two molecular units are contained in the unit cell. As shown in the projection of the structure onto the (010) planes (Fig. 2), BD and TCNQ molecules are alternately stacked along the c axis, orienting their molecular planes almost perpendicular to the axis, and their long molecular axes are in the [201] direction. The overlap of BD and TCNQ molecules in this crystal is of the type A shown as Fig. 3(a), having the average intermolecular separation of 3.24 Å, between BD and TCNQ. We measured the reflection spectrum as well as the transmission spectrum on the (010) face of this crystal.

The observed reflection spectra are shown in Fig. 4, and the absorption spectra directly observed by the transmission method are shown in Fig. 5 (solid lines). It should be noted in Fig. 5 that the absorption spectra obtained by the two entirely different experimental methods are in satisfactory agreement with each other. As we will show later, a similarly good agreement between the spectra obtained by the two methods could be found in all cases studied in the present study. This fact provides an evidence for the validity of the procedure which we have adopted for the measurement and analysis of reflectance data.

As shown in Fig. 5, the //c absorption spectrum exhibits a strong absorption band with a maximum at $7.4\times10^3$ cm$^{-1}$ and a shoulder at about $9\times10^3$

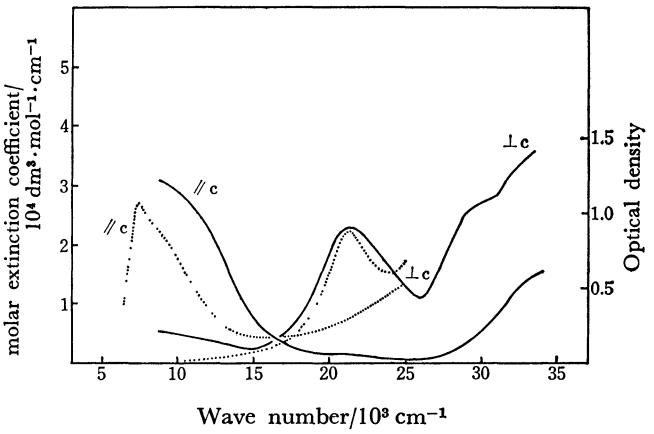


Fig. 5. Absorption spectra on the (010) plane of BD–TCNQ–[n]. The solid lines are the absorption spectra measured by the transmission method. The ordinate is optical density. The dotted lines are absorption spectra calculated by the reflection spectra. The ordinate is molar extinction coefficient.

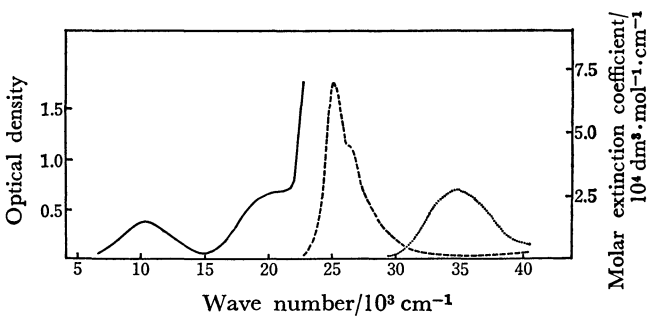


Fig. 6. Absorption spectra of BD (·····) and TCNQ (----) in the dichloromethane solution. The ordinate is molar extinction coefficient. Absorption spectra of BD–TCNQ complex (——) in the chloroform solution. The ordinate is optical density.

$cm^{-1}$. This infrared absorption band is strongly polarized in the c axis direction (BD–TCNQ stacking direction). On the other hand, the ⊥c spectrum shows an absorption band at $21.2\times10^3$ $cm^{-1}$, completely polarized in the [201] direction. The ⊥c spectrum measured by the transmission method shows another two absorption bands in the ultraviolet region, the one being at $29\times10^3$ $cm^{-1}$ and the other at above $33\times10^3$ $cm^{-1}$. Figure 6 shows the absorption spectra of BD and TCNQ molecules observed on their dichloromethane solutions, and the charge-transfer bands of the BD–TCNQ complex formed in the chloroform solution. The absorption spectrum of BD shows a broad absorption band in the region from $30\times10^3$ $cm^{-1}$ to $40\times10^3$ $cm^{-1}$ (the maximum is at $35\times10^3$ $cm^{-1}$). This band can be assigned mainly to the $\pi$-$\pi^*$ transition ($^1B_{3u}\leftarrow{}^1A_g$) polarized along the long molecular axis of BD. According to the molecular orbital calculation, there must be a weak absorption band associated with the short-axis polarized $\pi$-$\pi^*$ transition ($^1B_{2u}\leftarrow{}^1A_g$) in the same region. Seemingly, this weak band is hidden under the strong absorption band mentioned above. In the solution spectrum of TCNQ, the absorption band at $25.4\times10^3$ $cm^{-1}$ is due to the lowest $\pi$-$\pi^*$ transition ($^1B_{3u}\leftarrow{}^1A_g$), polarized in the long-axis direction. BD and TCNQ molecules form a stable charge-transfer (CT) complex in the chloroform solution. As shown in Fig. 6, this molecular complex exhibits the first CT band at $10.3\times10^3$ $cm^{-1}$ and the second one at $20\times10^3$ $cm^{-1}$. It was found in our previous study that the energy separation between the first and second CT bands was always about 1.3 eV in the solution spectra of a series of the molecular complexes which involve BD as the donor, irrespective of the acceptor, and the separation of the two CT bands is approximately equal to the energy difference between the highest and second highest occupied orbitals of BD. These facts indicate that the second CT band of the solution spectrum of BD–TCNQ complex is associated with the charge transfer from the second highest occupied molecular orbital (second HOMO) of BD to the lowest unoccupied molecular orbital (LUMO) of TCNQ, while the first CT band is associated with that from the HOMO of BD to the LUMO of TCNQ.

Let us compare the crystal spectrum of BD–TCNQ–[n] with the solution spectra discussed above. The $7.4\times10^3$ $cm^{-1}$ band of the //c spectrum undoubtedly corresponds to the first CT band of the solution spectrum of BD–TCNQ complex, although its shift, $3\times10^3$ $cm^{-1}$, to lower energy is a little larger than the shift usually found for a typical CT complex.

From the simple comparison of the crystal spectrum with the solution spectra of BD, TCNQ, and their complex, we could conclude that the $21.2\times10^3$ $cm^{-1}$ band of the crystal spectrum corresponds to the second CT band of the solution spectrum of BD–TCNQ complex, and the $29\times10^3$ $cm^{-1}$ band and the band above $33\times10^3$ $cm^{-1}$ are the local-excitation bands associated with the transitions in TCNQ and BD, respectively. However, it should be noted that the $21.2\times10^3$ $cm^{-1}$ band of the crystal spectrum is polarized perpendicular to the direction of the BD–TCNQ stack. This is unusual for a CT band. On the other hand, if the $21.2\times10^3$ $cm^{-1}$ band is due to the $^1B_{3u}\leftarrow{}^1A_g$ transition of TCNQ, we must consider that it is shifted by $4\times10^3$ $cm^{-1}$ to lower energy as compared with the solution spectrum.

A BD molecule overlaps with the adjacent TCNQ molecule, in the manner shown in Fig. 3(a). In this case, the overlap integral between the HOMO ($b_1$) of BD and the LUMO ($b_1$) of TCNQ is large, but the overlap integral between the second HOMO ($a_1$) of BD and the LUMO ($b_1$) of TCNQ must be zero. This means that the absorption band, which has been tentatively attributed to the charge transfer from the second HOMO of BD to the LUMO of TCNQ, cannot appear unless the above CT configurations is mixed with another excited configuration which gives a strong absorption band. The most probable mechanism would be the mixing of the local excitation associated with the lowest $\pi$-$\pi^*$ transition ($^1B_{3u}\leftarrow{}^1A_g$) of TCNQ. In order to confirm this idea, we carried out a molecular orbital calculation on the isolated BD–TCNQ pair of the geometry found in the crystal. The method of calculation is the same as the one which was previously used by Ohta, Kuroda, and Kunii for the molecular complexes of polycyclic aromatic hydrocarbon

TABLE 1. TRANSITIONS PREDICTED BY THE SCF·MO·CI CALCULATION ON A BD·TCNQ PAIR CORRESPONDING TO BD-TONQ-[n] CRYSTAL

| | Transition[a] | Wave number $\nu/10^3$ cm$^{-1}$ | $f$[b] | Transition dipole[c] | | | Character of transition | | | | Assignment |
|---|---|---|---|---|---|---|---|---|---|---|---|
| | | | | $M_x$ | $M_y$ | $M_z$ | $(DD)_m$ | $(AA)_m$ | $(DA)_m$ | $(AD)_m$ | |
| (1) | (16→17) | 12.51 | 0.356 | — | — | 1.619 | 0.13 | 0.13 | 0.69 | 0.03 | CT(D→A) |
| (2) | (15→17) | 17.55 | 0.802 | 2.052 | — | — | 0.08 | 0.38 | 0.43 | 0.07 | CT(D→A)+LE(A*) |
| (3) | (14→17) | 24.52 | 0.559 | 1.450 | — | — | 0.09 | 0.39 | 0.42 | 0.07 | CT(D→A)+LE(A*) |
| (4) | (16→19) | 26.96 | 0.124 | — | 0.651 | — | 0.00 | 0.19 | 0.75 | 0.00 | CT(D→A) |
| (5) | (16→20) | 28.07 | 0.196 | 0.802 | — | — | 0.01 | 0.20 | 0.77 | 0.01 | CT(D→A) |
| (6) | (15→20) | 31.22 | 0.018 | — | — | 0.235 | 0.00 | 0.46 | 0.50 | 0.00 | CT(D→A)+LE(A*) |
| (7) | (15→18) | 32.35 | 0.143 | — | 0.638 | — | 0.04 | 0.37 | 0.46 | 0.01 | CT(D→A)+LE(A*) |
| (8) | (16→21) | 33.91 | 0.494 | — | 1.157 | — | 0.06 | 0.15 | 0.56 | 0.04 | CT(D→A) |
| (9) | (16→22) | 34.21 | 1.850 | 2.233 | — | — | 0.80 | 0.01 | 0.01 | 0.15 | LE(D*) |

a) The main excitation is indicated here: $(i \rightarrow j)$ stands for the electron excitation from the $i$-th orbital to the $j$-th orbital. b) Oscillator strength. c) x and y are parallel to the long and short axes of BD and TCNQ; z axis is parallel to the direction connecting the centers of BD and TCNQ.

with tetracyanoethylene.[15] A $\pi$-orbital of a supermolecule, BD–TCNQ pair, is expressed by the linear combination of $2p_z$ AO's as follows.

$$\phi_i = \sum_{\mu=1}^{n_d+n_a} C_{i\mu}\phi_\mu \tag{5}$$

where $\phi_\mu$ with $\mu=1$—$n_d$ are the AO's associated with the donor and those with $\mu=n_d+1$—$n_d+n_a$ are the AO's associated with the acceptor. In order to see the contributions of the donor and acceptor for the $i$-th molecular orbital, we define $D_i$ and $A_i$ as follows.

$$D_i = \sum_{\mu=1}^{n_d} C_{i\mu}^2 \qquad A_i = \sum_{\mu=n_a+1}^{n_d+n_a} C_{i\mu}^2 \tag{6}$$

The $\pi$-orbital scheme calculated for the BD–TCNQ pair and those for the constituent molecules are illustrated in Fig. 7, where the values $(D_i, A_i)$ are given for each molecular orbital of BD–TCNQ pair. With the aid of $D_i$ and $A_i$ values and the symmetry consideration, we derived the correlation between the orbitals of BD–TCNQ pair and those of BD and TCNQ molecules as illustrated in Fig. 7 with dotted lines.

The excited states of BD–TCNQ pair were calculated by taking into account the configuration interaction of all singly-excited configurations. The results of this calculation are summarized in Table 1. The electronic transitions in a molecular pair DA can be classified into four categories: (a) the local excitation LE(D*) associated with a transition in the donor molecule D, (b) the local excitation LE(A*) associated with a transition in the acceptor molecule A, (c) the charge-transfer excitation CT(D→A), (d) the back charge-transfer excitation CT(A→D). The excitation of an electron from the $i$-th orbital to the $j$-th orbital of the molecular pair, $\Phi_{ij}$, generally has a character that LE(D*), LE(A*), CT(D→A), and CT(A→D) are mixed with the weights proportional to $D_iD_j$, $A_iA_j$, $D_iA_j$ and $A_iD_j$, respectively. When the CI (configuration interaction) wavefunction of the $m$-th excited state, $\Psi_m$, is expressed as,

$$\Psi_m = \sum_{ij} b_{ij,m}\Phi_{ij} \tag{7}$$

we define the following quantities.

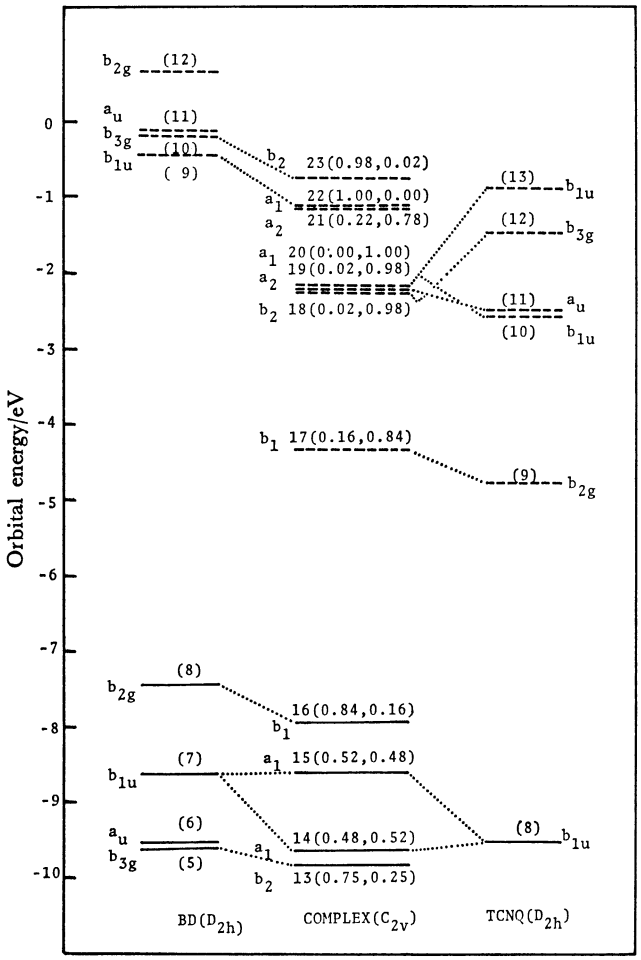


Fig. 7. Molecular orbitals of BD, TCNQ, and BD-TCNQ complex. The numerical values in the parenthesis correspond to the weight of the donor and acceptor character.

$$\begin{aligned}(DD)_m &= \sum_{ij} b^2_{ij,m}D_iD_j \\ (AA)_m &= \sum_{ij} b^2_{ij,m}A_iA_j \\ (DA)_m &= \sum_{ij} b^2_{ij,m}D_iA_j \\ (AD)_m &= \sum_{ij} b^2_{ij,m}A_iD_j\end{aligned} \tag{8}$$

The values of $(DD)_m$, $(AA)_m$, $(DA)_m$, and $(AD)_m$ give the weights of the characters of LE(D*), LE(A*), CT(D→A), and CT(A→D) in the $m$-th excited state, respectively. The above values of each transition are also given in Table 1. For example, in the case of the transition (1) which is predicted at $12.51\times10^3$ $cm^{-1}$, the $(DA)_m$ value is about 0.7, which indicates that this transition is mainly associated with a charge transfer from BD to TCNQ. In effect, the transition moment is predicted to be in the direction connecting the centers of BD and TCNQ molecules. The result for the transition (2) is most interesting. This transition is predicted to have its transition moment parallel to the long axes of BD and TCNQ molecules. In this case, $(DA)_m$ is 0.43 and $(AA)_m$ is 0.38. This means that the transition has a character that CT (D→A) and LE(A*) are mixed with almost equal weights. The same can be said for the third transition predicted at $24.52\times10^3$ $cm^{-1}$. When we calculate the transitions in TCNQ molecule using the same method, the lowest $\pi$-$\pi^*$ transition ($^1B_{3u}\leftarrow{}^1A_g$) is predicted at $22.18\times10^3$ $cm^{-1}$, which is lower by about $3\times10^3$ $cm^{-1}$ than the experimental value. From the comparison of the results of the calculation on BD–TCNQ pair and those on TCNQ molecule, we can conclude that the CT configuration associated with the charge transfer from the second HOMO of BD to the LUMO of TCNQ and the LE(A*) configuration associated with the lowest singlet $\pi$-$\pi^*$ excitation of TCNQ, are strongly mixed with each other in BD–TCNQ pair to give the transitions (2) and (3).

Although the crystal of BD–TCNQ–[n] is not composed of isolated BD–TCNQ pairs, the results of the above calculation can be used to interprete the crystal spectrum, since the main features of the crystal spectrum of a CT complex is determined by the interaction between neighboring donor and acceptor molecules. The z and x axes in Table 1 correspond to the //c and ⊥c directions of the crystal of BD–TCNQ–[n], respectively. Consequently, the transition (1) which is predicted to be polarized in the z axis direction will appear in the //c spectrum, while the x axis polarized transitions, (2), (3), (5), and (9) are expected to appear in the ⊥c spectrum. Therefore, we can assign the $7.4\times10^3$ $cm^{-1}$ band in the //c spectrum to the transition (1), and the $21.2\times10^3$ $cm^{-1}$ and $29\times10^3$ $cm^{-1}$ bands in the ⊥c spectrum to the transitions (2) and (3), respectively. The strong absorption band at above $33\times10^3$ $cm^{-1}$ in the ⊥c spectrum is likely to correspond to the transition (9) which is mainly associated with the lowest $\pi$-$\pi^*$ transition of BD. We were not able to observe any absorption maximum corresponding to the transition (5). Seemingly, it is hidden under the strong absorption bands corresponding to the transitions (3) and (9).

The low frequency dielectric constants of the microcrystalline powders of molecular complexes were studied by Ishii *et al.*[16] by use of the microwave cavity perturbation method. It was revealed that the observed dielectric constants are always larger than the values estimated under the assumption that the molecular polarization of a complex is equal to the simple sum of the molecular polarizations of the

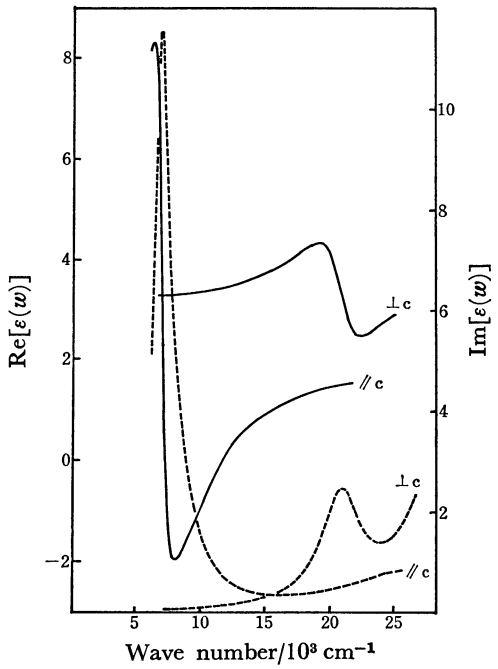


Fig. 8. The real (——) and the imaginary (----) parts of the dielectric function of BD–TCNQ–[n].

constituent molecules. The dielectric constant of the BD–TCNQ–[n] powder is 6—7 according to the above paper. If we estimate the molecular polarization of BD–TCNQ system as the simple sum of the molecular polarizations of BD and TCNQ, and assume the Clausius-Mossotti equation, the dielectric constant of BD–TCNQ–[n] is estimated to be about 4, which is smaller by 2—3 than the observed dielectric constant. This difference must be due to the enhancement of dielectric constant by the intermolecular interaction. It is most likely that the above enhancement arises mainly from the CT interaction between BD and TCNQ. To confirm this idea, we carried out the following analysis.

Fig. 8 shows the real and imaginary parts of the frequency-dependent dielectric functions obtained from the //c and ⊥c reflection spectra. The static dielectric constant $\varepsilon(0)$ can be estimated from the complex dielectric function $\varepsilon(\omega)$ by means of the Kramers-Kronig equation for an insulator.

$$\varepsilon(0) = 1 + \frac{2}{\pi}\int_0^\infty \frac{\mathrm{Im}\varepsilon(\omega)}{\omega}d\omega \qquad (9)$$

According to this relation, the contribution of the CT transitions to $\varepsilon(0)$ can be expressed as follows.

$$\Delta\varepsilon(\mathrm{CT}) = \frac{2}{\pi}\int_{\omega_1}^{\omega_2} \frac{\mathrm{Im}\varepsilon(\omega)}{\omega}d\omega \qquad (10)$$

where $\omega_1$ and $\omega_2$ are the low- and high-frequency limits of the region of CT band. Taking $\omega_1=4\times10^3$ $cm^{-1}$ and $\omega_2=24\times10^3$ $cm^{-1}$, we performed the above integration using the complex dielectric functions obtained from the //c and ⊥c reflection spectra. The $\Delta\varepsilon$(CT) value thus calculated was 3.0 and 0.5 for the //c and ⊥c polarizations, respectively. The $\Delta\varepsilon$ (CT) value must be zero for the //b polarization since the CT transitions concerned here has no //b component. In order to compare with the dielectric behavior

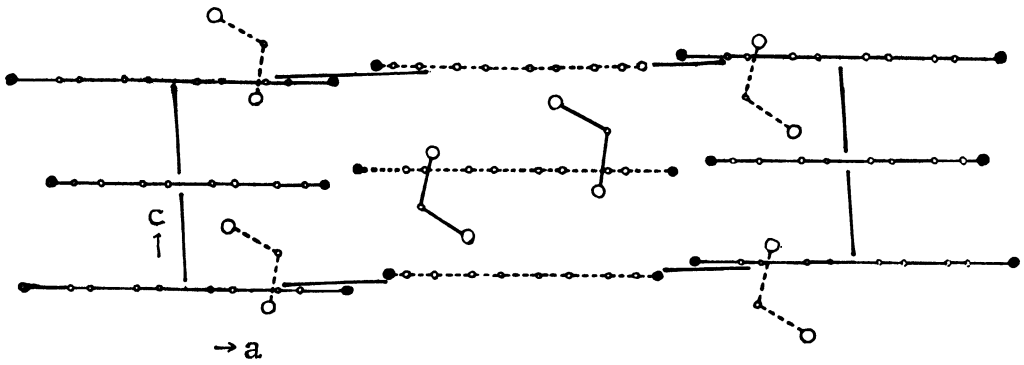


Fig. 9. The crystal structure of BD–TCNQ–[$CH_2Cl_2$] projected onto the (010) plane.

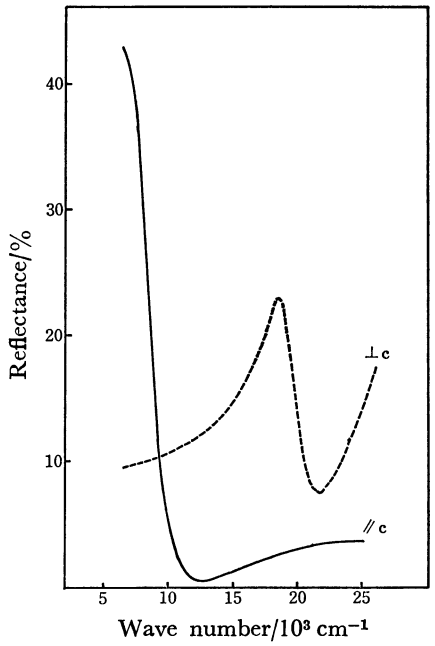


Fig. 10. Reflection spectra on the (010) plane of BD–TCNQ–[$CH_2Cl_2$].

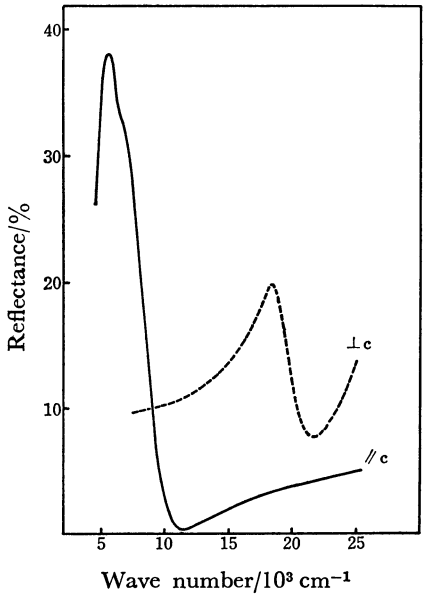


Fig. 11. Reflection spectra on the (100) plane of BD–TCNQ–[$CH_2BrCH_2Br$].

of the microcrystalline powder, we have to take the average of the $\Delta\varepsilon$(CT) values for the three polarizations. This average value is calculated to be 1.2. Although it is a little smaller than the enhancement of dielectric constant, estimated from the data by the microwave cavity perturbation method, the above result indicates that the enhancement of dielectric constant is indeed mainly due to the intermolecular charge-transfer interaction.

*BD–TCNQ–[$CH_2Cl_2$] and BD–TCNQ–[$CH_2BrCH_2Br$].* The crystal of BD–TCNQ–[$CH_2Cl_2$] is monoclinic, with the space group I2/m. The lattice constants are $a$=20.892 Å, $b$=9.950 Å, $c$=6.445 Å, and $\beta$=91.92°.[3] Two molecular units are contained in the unit cell as shown in Fig. 9. The BD and TCNQ molecules are alternately stacked along the c axis to form a BD–TCNQ column, in which the molecular overlap of BD and TCNQ are almost the same as that in BD–TCNQ–[n] except that the average separation of the molecular planes, 3.22 Å, is a little smaller than that in the latter. The main difference between BD–TCNQ–[$CH_2Cl_2$] and BD–TCNQ–[n] is that, in the former crystal, there are channels surrounded by four BD–TCNQ columns, in which dichloromethane molecules are included, while BD–TCNQ columns are closely packed in the crystal of BD–TCNQ–[n]. The adjacent BD–TCNQ columns in BD–TCNQ–[$CH_2Cl_2$] are connected with each other by the intermolecular hydrogen bonds between C≡N group of TCNQ and $NH_2$ group of BD. These hydrogen bonds seem to contribute to the stabilization of the channeled structure of BD–TCNQ sublattice of the solvated modification.

The crystal of BD–TCNQ–[$CH_2BrCH_2Br$] is orthorhombic with the space group Immm. The lattice constants are $a$=10.205 Å, $b$=20.785 Å, and $c$=6.525 Å. The a and b axes in this crystal correspond to the b and a axes of BD–TCNQ–[$CH_2Cl_2$], respectively, and the structure of BD–TCNQ sub-lattice is almost the same as that of the latter crystal, except that the average separation between the molecular planes of BD and TCNQ is 3.26 Å.

The reflection spectrum measured on the (010) face of BD–TCNQ–[$CH_2Cl_2$] and that measured on the corresponding crystal face, (100), of BD–TCNQ–[$CH_2BrCH_2Br$] are shown in Fig. 10 and Fig. 11, respectively. From the analyses of these spectra, we obtained the absorption spectra shown in Figs. 12 and 13. In Fig. 12, we have also shown the absorption

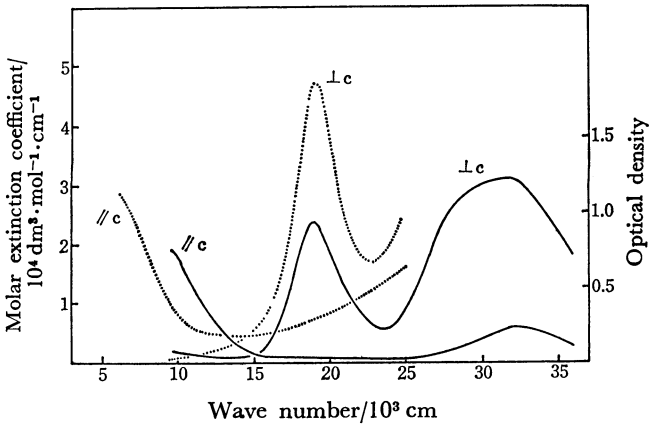


Fig. 12. Absorption spectra on the (010) plane of BD-TCNQ-[$CH_2Cl_2$]. The continuous lines are the absorption spectra measured by transmission method. The ordinate is optical density. The dotted lines are absorption spectra calculated by the reflection spectra. The ordinate is molar extinction coefficient.

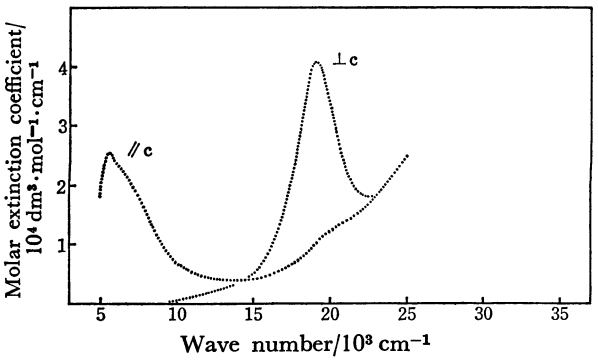


Fig. 13. Absorption spectra on the (100) plane of BD-TCNQ-[$CH_2BrCH_2Br$] calculated by the reflection spectra. The ordinate is molar extinction coefficient.

spectrum measured on the same crystal face directly by the transmission experiment.

The spectra of BD-TCNQ-[$CH_2Cl_2$] and BD-TCNQ-[$CH_2BrCH_2Br$] are very similar to each other as we can expect from the similarity of BD-TCNQ sub-lattice in these two crystal forms. In both cases, the //c spectrum exhibits a strong absorption band in the near-infrared region. The maximum of this band is located at $5.7\times10^3$ cm$^{-1}$ in the case of BD-TCNQ-[$CH_2BrCH_2Br$]. Seemingly the absorption maximum is at almost the same wave number in the case of BD-TCNQ-[$CH_2Cl_2$]. This infrared band is the CT band corresponding to the $7.4\times10^3$ cm$^{-1}$ band of BD-TCNQ-[n]. There are three absorption bands in the ⊥c spectrum: a relatively sharp one at $19.0\times10^3$ cm$^{-1}$ and two broad ones at $27\times10^3$ and $32\times10^3$ cm$^{-1}$, respectively. These bands must correspond to the absorption bands observed at $21.2\times10^3$, $29\times10^3$, and above $33\times10^3$ cm$^{-1}$, respectively, in the ⊥c spectrum of BD-TCNQ-[n]. It should be noted that all absorption bands are shifted to lower wave number by about $2\times10^3$ cm$^{-1}$ in the spectrum of BD-TCNQ-[$CH_2Cl_2$] as compared with the spectrum of BD-TCNQ-[n], and the intensity of $19.0\times10^3$ cm$^{-1}$ band is markedly enhanced in the solvated modifications.

We carried out the molecular orbital calculation on the BD-TCNQ pair taking the separation of the molecular planes as 3.22 Å as in the crystal of BD-TCNQ-[$CH_2Cl_2$]. This calculation shows that the transitions which are responsible for the observed absorption bands, are shifted to lower wave number on decreasing the molecular separation from 3.24 Å to 3.22 Å. But the predicted shift is 50 and 300 cm$^{-1}$ for the transitions (1) and (2), respectively, and 600 cm$^{-1}$ for the transitions (3) and (8) of Table 1. These

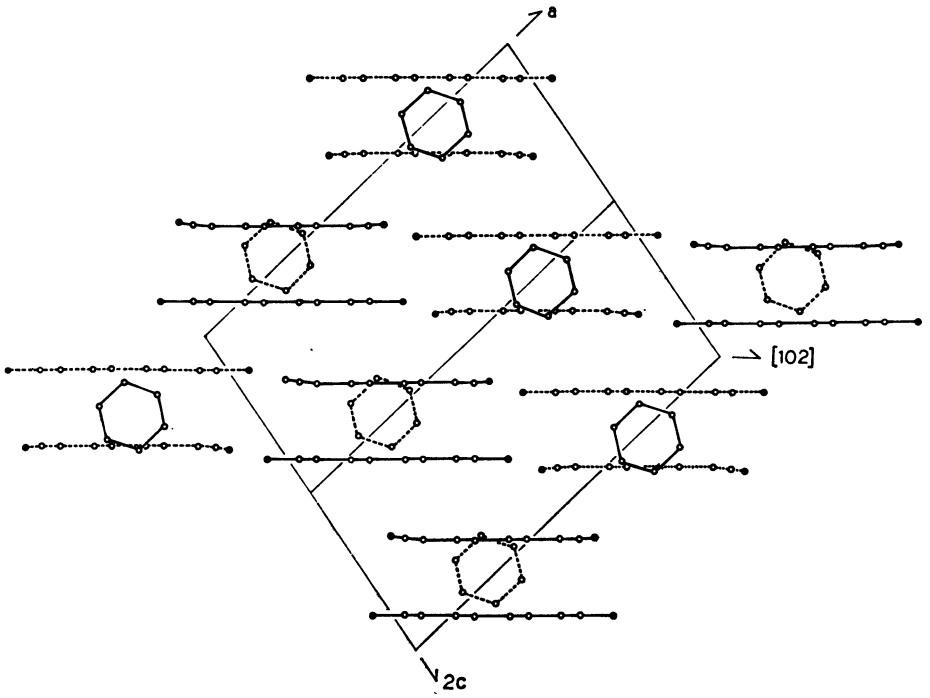


Fig. 14. The crystal structure of BD-TCNQ-[$C_6H_6$] projected onto the (010) plane.

TABLE 2. TRANSITION PREDICTED BY SCF·MO·CI CALCULATIONS ON THE TWO STRUCTURES OF BD·TCNQ PAIR CORRESPONDING TO BD-TCNQ-[$C_6H_6$]; SEE Fig. 3 (a) AND (b) FOR THE OVERLAPPING OF BENZIDINE AND TCNQ IN EACH MODEL

| | Transition | Wave number $\nu/10^3$ cm$^{-1}$ | $f$ | Transition dipole | | | Charabter of transition | | | | Assignment |
|---|---|---|---|---|---|---|---|---|---|---|---|
| | | | | $M_x$ | $M_y$ | $M_z$ | $(DD)_m$ | $(AA)_m$ | $(DA)_m$ | $(AD)_m$ | |
| Model (a) | | | | | | | | | | | |
| (1) | (16→17) | 13.83 | 0.467 | — | — | 1.762 | 0.18 | 0.18 | 0.56 | 0.06 | CD(D→A) |
| (2) | (15→17) | 17.35 | 0.964 | 2.263 | — | — | 0.11 | 0.40 | 0.34 | 0.12 | CT(D→A)+LE(A*) |
| (3) | (14→17) | 24.98 | 0.266 | 0.989 | — | — | 0.08 | 0.49 | 0.28 | 0.12 | LE(A*) |
| (4) | (16→19) | 28.21 | 0.144 | — | 0.685 | — | 0.02 | 0.26 | 0.69 | 0.01 | CT(D→A) |
| (5) | (16→20) | 29.08 | 0.244 | 0.898 | — | — | 0.02 | 0.27 | 0.67 | 0.02 | CT(D→A) |
| (6) | (15→20) | 30.77 | 0.023 | — | — | 0.262 | 0.03 | 0.46 | 0.46 | 0.04 | CT(D→A)+LE(A*) |
| (7) | (15→18) | 30.79 | 0.166 | — | 0.705 | — | 0.03 | 0.46 | 0.43 | 0.01 | CT(D→A)+LE(A*) |
| (8) | (15→19) | 31.96 | 0.102 | — | 0.542 | — | 0.04 | 0.46 | 0.42 | 0.02 | CT(D→A)+LE(A*) |
| (9) | (16→21) | 33.22 | 1.663 | 2.148 | — | — | 0.72 | 0.00 | 0.02 | 0.23 | LE(D*) |
| (10) | (16→22) | 33.56 | 0.295 | — | 0.900 | — | 0.27 | 0.19 | 0.47 | 0.09 | CT(D→A) |
| Model (b) | | | | | | | | | | | |
| (1′) | (16→17) | 10.16 | 0.505 | 1.595 | — | 1.429 | 0.13 | 0.10 | 0.73 | 0.02 | CT(D→A) |
| (2′) | (15→17) | 20.47 | 0.230 | 0.788 | — | 0.642 | 0.09 | 0.29 | 0.53 | 0.05 | CT(D→A) |
| (3′) | (14→17) | 21.32 | 1.159 | 2.210 | — | 0.358 | 0.06 | 0.54 | 0.29 | 0.09 | LE(A*) |
| (4′) | (16→19) | 25.98 | 0.427 | 1.224 | — | 0.131 | 0.00 | 0.14 | 0.82 | 0.00 | CT(D→A) |
| (5′) | (16→20, 21, 23) | 31.40 | 0.230 | — | 0.823 | — | 0.23 | 0.09 | 0.55 | 0.05 | CT(D→A) |
| (6′) | (16→22) | 32.19 | 1.196 | 1.840 | — | 0.199 | 0.81 | 0.03 | 0.02 | 0.11 | LE(D*) |
| (7′) | (16→25 / 14→18) | 35.86 | 0.506 | — | 1.141 | — | 0.30 | 0.40 | 0.22 | 0.00 | LE(A*)+LE(D*) |

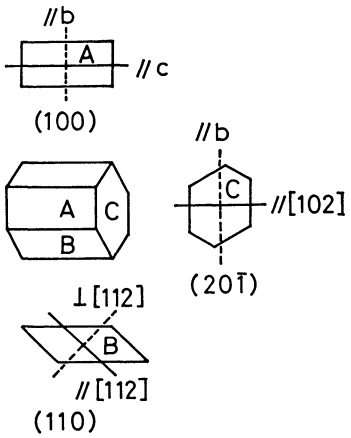


Fig. 15. Crystal morphology and principal axis directions for BD-TCNQ-[$C_6H_6$] single crystal.

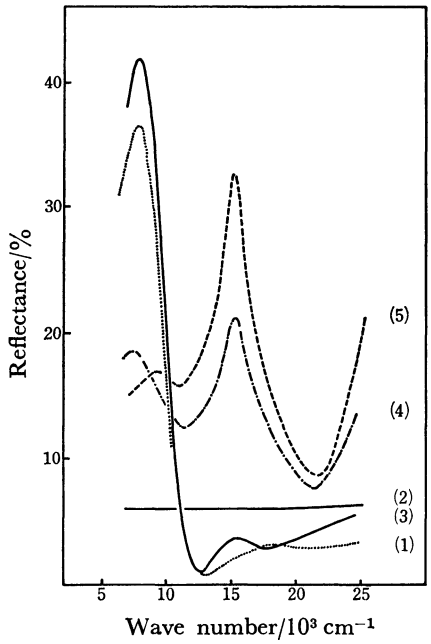


Fig. 16. Reflection spectra of BD-TCNQ-[$C_6H_6$]. The numbers correspond to the spectra polarized to (1) //c on the (100) (2) //b on the (100) (3) ⊥[112] on the (110) (4) //[112] on the (110) (5) //[102] on the (201).

are too small to explain the observed difference between the spectra of BD-TCNQ-[$CH_2Cl_2$] and BD-TCNQ-[n]. The oscillator strength of the transition (2) is predicted to increase only by about 15 percent on decreasing the molecular separation from 3.24 Å to 3.22 Å, while the observed oscillator strength of the $19.0\times10^3$ cm$^{-1}$ band of BD-TCNQ-[$CH_2Cl_2$] is almost twice that of the $21.2\times10^3$ cm$^{-1}$ band of BD-TCNQ-[n]. Thus, the observed differences between the spectra of BD-TCNQ-[$CH_2Cl_2$] and BD-TCNQ-[n] cannot be simply explained from the decrease of the intermolecular separation. Seemingly, it is necessary to take into account the effects of the intermolecular hydrogen bonds and the presence of solvent molecules in order to fully understand the observed differences.

*BD-TCNQ-[$C_6H_6$].* The crystal of BD-TCNQ-[$C_6H_6$] is monoclinic with the space group $P2_1/m$, the lattice constants being $a=17.184$ Å, $b=9.852$ Å, $c=7.680$ Å, and $\beta=100.3°$.[5] The unit cell contains two molecular units. The structure of BD-TCNQ sub-lattice in this crystal is quite different from

Table 3. Comparison between the predicted and observed absorption bands in the //c and //b spectra of the (100) plane of BD-TCNQ-[$C_6H_6$]

| //c Spectrum | | | | | //b Spectrum | | | | |
|---|---|---|---|---|---|---|---|---|---|
| $\nu/10^3$ cm$^{-1}$ | $f_c$[a] | | Ttansition[c] | observed band $\nu/10^3$ cm$^{-1}$ | $\nu/10^3$ cm$^{-1}$ | $f_b$[b] | | Transition[c] | Observed band $\nu/10^3$ cm$^{-1}$ |
| 10.16 | 0.48 | (1′) | CT(D→A) | 4—15 (max. 7.5) | | | | | |
| 13.83 | 0.20 | (1) | CT(D→A) | | | | | | |
| 17.35 | 0.32 | (2) | CT(D→A)+LE(A) | 15—24 (max. 17.3 shoulder: 20) | | | | | |
| 20.47 | 0.21 | (2′) | CT(D→A) | | | | | | |
| 21.32 | 0.22 | (3′) | LE(A*) | | | | | | |
| 24.98 | 0.09 | (3) | LE(A*) | >25 | 28.21 | 0.14 | (4) | CT(D→A) | 25—30 |
| 25.98 | 0.10 | (4′) | CT(D→A) | | 30.79 | 0.17 | (6) | CT(D→A)+LE(A*) | |
| 29.08 | 0.08 | (5) | CT(D→A) | | 31.40 | 0.23 | (5′) | CT(D→A) | |
| 32.19 | 0.28 | (6′) | LE(D*) | | 31.96 | 0.10 | (8) | CT(D→A)+LE(A*) | |
| 33.22 | 0.05 | (9) | LE(D*) | | 33.56 | 0.30 | (10) | CT(D→A) | ≈33 |
| | | | | | 35.86 | 0.51 | (7′) | LE(A*)+LE(D*) | |

a) //c component of oscillator strength predicted for each transition. //b component of oscillator strength predicted for each transition. c) Refer Table 2 for the numberings of transitions.

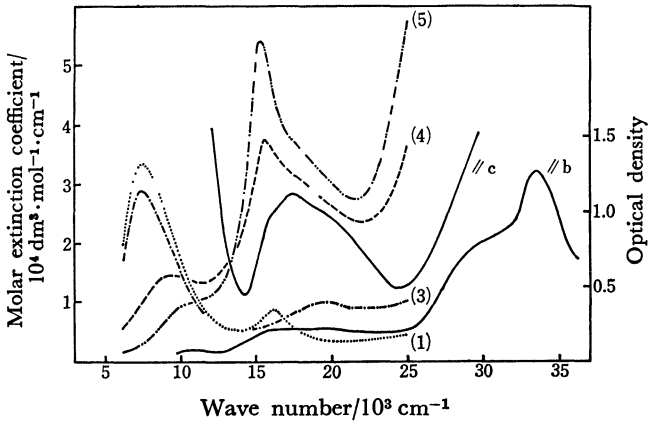


Fig. 17. Absorption spectra of BD-TCNQ-[$C_6H_6$]. The continuous lines are the absorption spectra on the (100) plane measured by the transmission method. The ordinate is optical density. The other lines are the absorption spectra calculated by the reflection spectra. The ordinate is molar extinction coefficient. The numbers correspond to those in Fig. 16.

Table 4. Comparison between the observed and predicted oscillator strength of BD-TCNQ-[$C_6H_6$]

| | Spectrum[a] | | | | |
|---|---|---|---|---|---|
| | (1) | (2) | (3) | (4) | (5) |
| [Infrared band] | | | | | |
| $\nu_m/10^3$ cm$^{-1}$ | 7.5 | — | 7.5 | 9.4 | ≈10 |
| $f_{obsd}$[b] | 1.2 | 0.0 | 0.9 | 0.7 | 0.2 |
| $f(1)$ | 0.308 | 0.000 | 0.427 | 0.000 | 0.000 |
| $f(1')$ | 0.476 | 0.000 | 0.256 | 0.242 | 0.296 |
| $f(1)+f(1')$ | 0.784 | 0.000 | 0.683 | 0.242 | 0.296 |
| [Visible band] | | | | | |
| $\nu_m/10^3$ cm$^{-1}$ | 16.1 | — | 19.5 | 15.6 | 15.3 |
| $f_{obsd}$[b] | 0.1 | 0.0 | 0.2 | 2.1 | 2.8 |
| $f(2)$ | 0.334 | 0.000 | 0.015 | 0.789 | 0.964 |
| $f(2')$ | 0.211 | 0.000 | 0.106 | 0.119 | 0.145 |
| $f(3')$ | 0.207 | 0.000 | 0.003 | 0.914 | 1.117 |
| $f(2)+f(2')+f(3')$ | 0.752 | 0.000 | 0.124 | 1.822 | 2.226 |

a) The numbers of the spectrum correspond to those in Fig. 17. b) $f_{obsd}$ is the oscillator strength obtained from each reflection spectrum. $f(a)$ is the projected value of the predicted oscillator strength of the transition ($a$) on each observed polarization-direction.

the cases discussed above. The BD–TCNQ sub-lattice is definitely composed of BD–TCNQ pairs (see Fig. 14). The molecular overlap within the BD–TCNQ pair is of the same type as those in BD–TCNQ-[n] and BD-TCNQ-[$CH_2Cl_2$], which are shown in Fig. 3(a), but with a very short intermolecular separation of 3.09 Å. On the other hand, the BD–TCNQ overlap between the adjacent pairs is of the type shown in Fig. 3(b) with an intermolecular separation of 3.27 Å. Here again, the hydrogen bonds between C≡N group of TCNQ and $NH_2$ group of BD stabilize the channeled structure of the BD–TCNQ sub-lattice.

The typical shape of the crystal of BD–TCNQ-[$C_6H_6$] is a hexagonal prism with the developed crystal faces (100), (110), and (201) as shown in Fig. 15. The reflection spectra were measured on all of the above three crystal faces. Fig. 16 shows the observed spectra. The spectra (1) and (2) were obtained on the (100) face for the light polarizations parallel to the c and b axes, respectively; the spectra (3) and (4) were obtained on the (110) face for the polarizations parallel and perpendicular to the [112] direction; the spectrum (5) is the one obtained on the (201) face for the polarization parallel to the [102] direction. The spectrum (1) shows two reflectance maxima at $7.6\times10^3$ and $15.5\times10^3$ cm$^{-1}$, while the spectrum (2) exhibits no indication of dispersion in the whole observed range. The spectra (3) and (4) also exhibit a reflectance maximum at about $7.6\times10^3$ cm$^{-1}$, but the spectrum (5) shows a small maximum at $9.0\times10^3$ cm$^{-1}$ instead of $7.6\times10^3$ cm$^{-1}$. This fact indicates that there are two kinds of transitions in the infrared region. In the visible region, the spectra (1), (4), and (5) exhibit a reflectance maximum at $15.5\times10^3$ cm$^{-1}$, but the spectrum (3) shows a maximum at $19\times10^3$ cm$^{-1}$. We note

also in the spectra (4) and (5), the shape of the reflectance curve at the high energy side of the $15.5\times10^3$ $cm^{-1}$ maximum suggests the presence of another dispersion.

The absorption spectra obtained by the analysis of the reflectance data are shown in Fig. 17, together with the absorption spectra directly observed by the transmission experiment on the (100) plane of the relatively thick crystal.

We carried out the molecular orbital calculations on the two models of BD–TCNQ pair corresponding to the two kinds of BD–TCNQ molecular overlap in BD–TCNQ–[$C_6H_6$]. The model (a) is the one corresponding to the arrangement of BD and TCNQ molecules within the BD–TCNQ pair and the model (b) is the one corresponding to that between adjacent pairs. The transitions which are predicted for the two models are listed in Table 2. Since the short molecular axis of TCNQ has been taken as the y axis direction in the above Table, the transition polarized in the y axis direction are expected to appear only in the //b spectrum, while other transitions are expected to have their transition moments within the (010) plane. Thus the comparison of the observed absorption band with the predicted transitions can be made as shown in Table 3. As indicated in this table, it is most likely that the absorption bands in the infrared region is associated with the transitions (1) and (1′), and those in the visible region are associated with the transitions (2), (2′), and (3′). Using the predicted oscillator strengths and the crystal structure data, we estimated the components of the oscillator strengths parallel to the polarization direction of each observed spectrum. The results are listed in Table 4 together with the observed values. Naturally it is difficult to expect a good quantitative agreement between the experimental and predicted values. But the general features of the absorption spectra can be understood from the results of the calculation. The results shown in Table 4 suggest that the absorption band at about $9\times10^3$ $cm^{-1}$ observed in the spectra (4) and (5) of Fig. 17 is the one associated with the transition (1′), while the strong infrared band in the spectra (1) and (3), is due to the superimposition of the bands associated with the transitions (1) and (1′). This means that the absorption band corresponding to the transition (1) is located at about $7\times10^3$ $cm^{-1}$, and is energetically lower than the one corresponding to the transition (1′), although the transition (1′) is predicted to be energetically lower than the transition (1), according to the calculation on the models of isolated BD–TCNQ pair. For the visible region, we can conclude that the weak absorption band at $19\times10^3$ $cm^{-1}$ in the spectrum (3) is due to the transition (2′), while, in the spectra (4) and (5), the strong peak at $15.5\times10^3$ $cm^{-1}$ is associated with the transition (2) and its high-energy tail is associated with the transition (3′). There exists a discrepancy as regards the spectral shape in the visible region between the spectrum (1) and the absorption spectrum measured directly by the transmission method on the same crystal plane (100). In this case, the absorption spectrum derived from the reflectance data seems to be less reliable since the reflectance of the (100) face in the above region is very small for the //c polarization, so that there could be relatively large errors in the process of their analysis. We consider that the absorption spectrum directly observed on a thick crystal is more reliable in this case than the spectrum derived from the reflectance data. The former shows a weak and broad visible absorption band with an indication that it is actually composed of three transitions. Indeed this is consistent with the results of calculation shown in Table 4.

*Summary and Conclusion.* In the present study, we have observed the absorption and reflection spectra on the known crystallographic faces of the single crystals of BD–TCNQ–[n], BD–TCNQ–[$CH_2Cl_2$], BD–TCNQ–[$CH_2BrCH_2Br$], and BD–TCNQ–[$C_6H_6$]. Usually in the case of the direct measurement of absorption spectrum by the transmission experiment with a microspectrophotometer, there remains some ambiguity as regards the identification of the crystallographic nature of the observing crystal face since it is hard to identify it directly by X-ray diffraction. On the other hand, in the case of the measurement of reflection spectrum by the microspectrophotometric technique, we can use a relatively large crystal, so that we can directly determine the observing crystal face by means of the X-ray diffraction, and it is also possible to observe the reflection spectrum on several different crystal faces. Thus we can determine the direction of the transition moment of an absorption band without any ambiguity. By this method, we confirmed that the first absorption band at about 6—$8\times10^3$ $cm^{-1}$ is polarized in the direction of BD–TCNQ stack, but the second absorption band at about $17\times10^3$ $cm^{-1}$ is polarized parallel to the direction of the long molecular axes of BD and TCNQ in the cases of BD–TCNQ–[n], BD–TCNQ–[$CH_2Cl_2$], and BD–TCNQ–[$CH_2BrCH_2Br$]. The situation is a little complicated in the case of BD–TCNQ–[$C_6H_6$]. The transmission experiment was possible only on the (100) face of the crystal of this modification, and the observed absorption spectra indicated that both the first and second band appear in the //c spectrum. However, by examining the reflection spectra obtained on three different crystal faces, we revealed that there exist two absorption bands of different polarizations in the infrared region, and three bands in the visible region. We carried out molecular-orbital calculations on the models of BD–TCNQ pair, and showed that the observed spectra can be satisfactorily interpreted by using the results of these calculations. It has been thus concluded that, in BD–TCNQ complexes, the infrared absorption band is associated with the charge transfer from the HOMO of BD to the LUMO of TCNQ, but the second CT excitation associated with the charge transfer from the second HOMO of BD to the LUMO of TCNQ is strongly mixed with the local excitation from the HOMO to the LUMO of TCNQ to give a visible absorption band and an absorption band at about $29\times10^3$ $cm^{-1}$. This can be understood as follows from the consideration of the orbital symmetries. BD and TCNQ molecules overlap on each other as shown in Fig. 3(a), having their molecular axes exactly on each

TABLB 5. OBSERVED OSCILLATOR STRENGTHS OF THE CHARGE-TRANSFER BANDS OF BD-TCNQ COMPLEXES

| | CT1 | | CT2[a] | | Intermolecular spacing | |
|---|---|---|---|---|---|---|
| | $\nu_{max}/10^3$ cm$^{-1}$ | $f$ | $\nu_{max}/10^3$ cm$^{-1}$ | $f$ | Å | |
| BD-TCNQ-[n] | 7.4 | 0.8 | 21.3 | 0.7 | 3.24 | |
| BD-TCNQ-[$CH_2Cl_2$] | <6.2 | (0.8) | 19.1 | 1.6 | 3.22 | H-bond |
| BD-TCNQ-[$CH_2BrCH_2Br$] | 5.7 | 0.8 | 19.8 | 1.5 | 3.26 | H-bond |
| BC-TCNQ-[$C_6H_6$] (a) | 7.5 | ≈1.2 | 15.3 | (<2.8)[b] | 3.09 | H-bond |
| (b) | ≈10 | | 19.5 | | 3.29 | |

a) This is not a pure charge-transfer band. Refer the text for the nature of this band. b) The contribution of the transition (3′) is included in this value.

other. As shown in Fig. 7, the HOMO of TCNQ and the second HOMO of BD have the same orbital symmetry $b_{1u}$. Therefore, the electronic excitations from these orbitals to the LUMO ($b_{2g}$) of TCNQ belong to the same symmetry, and can strongly mix with each other. On the other hand, because of the above orbital symmetries, the overlap integral between the second HOMO of BD and the LUMO of TCNQ must be zero. Thus the moments of the optical transition where the above two excitations are mixed, will be entirely due to the contribution of the excitation from the HOMO to the LUMO of TCNQ. This is the reason why the visible absorption band, which was tentatively considered as the second CT band in our previous study, is polarized perpendicular to the direction of BD–TCNQ stack.

We noted that the CT bands are very strong in the crystal spectra of BD–TCNQ complex as compared with the crystals of typical CT complexes such as pyrene–TCNE. From the analysis of reflectance data, we can determine the absolute oscillator strength of each absorption band. The values thus determined are given in Table 5. It should be noted that the oscillator strength of the first CT band is as large as 0.8. Interestingly, this is about twice the oscillator strength predicted for a BD–TCNQ pair by the molecular orbital calculations. The experimentally determined oscillator strength is much larger for the second CT band. This is primarily due to the effect of the mixing of the local excitation associated with the strong $^1B_{3u}\leftarrow{}^1A_g$ transition of TCNQ.

Finally, we wish to point out that, when dichloromethane or dibromoethane is included in the BD–TCNQ lattice, the absorption bands are shifted to lower energy by about $2\times10^3$ cm$^{-1}$. Since the strucuture within the BD–TCNQ stack remains almost the same except a slight change of the intermolecular separation, the above shifts must be due to the effect of included solvent molecules and/or to that of the formation of intermolecular hydrogen bonds.

We wish to thank Dr. T. Ohta in our laboratory for helping us to use his computer program for the molecular orbital calculation of supermolecule system.

We are grateful to Olympus Optical Co., Ltd. for their generous offer of Olympus MMSP-RK used in this study.

## References

1) T. Amano, H. Kuroda, and H. Akamatsu, *Bull. Chem. Soc. Jpn.*, **42**, 671 (1969).
2) H. Ohmasa, M. Kinoshita, and H. Akamatsu, *Bull. Chem. Soc. Jpn.*, **44**, 391, 395 (1971).
3) I. Ikemoto, K. Chikaishi, K. Yakushi, and H. Kuroda, *Acta Crystallogr., Sect. B.*, **28**, 3502 (1972).
4) K. Yakushi, I. Ikemoto, and H. Kuroda, *Acta Crystallogr., Sect. B*, **30**, 835 (1974).
5) K. Yakushi, I. Ikemoto, and H. Kuroda, *Acta Crystallogr., Sect. B*, **30**, 1738 (1974).
6) N. Takahashi, K. Yakushi, K. Ishii, and H. Kuroda, *Bull. Chem. Soc. Jpn.*, **49**, 182 (1976).
7) H. Kuroda, T. Kunii, S. Hiroma, and H. Akamatsu, *J. Mol. Spectrosc.*, **22**, 1 (1967).
8) For the method of calculation, see, for example, the following reference. F. Stern, "Elementary Theory of the Optical Properties of Solids," *Solid State Phys.*, **15**, 299 (1963).
9) H. W. Verleur, *J. Opt. Soc. Am.*, **58**, 1356 (1968).
10) I. H. Malison, *J. Opt. Soc. Am.*, **52**, 1377 (1962).
11) The single crystal of saphire were mounted on the small vessel in which 1-chloronaphthalene mixed with the powder of active charcoal was filled in order to avoid the reflection from the back surface of the crystal.
12) D. M. Roessler, *Brit. J. Appl. Phys.*, **16**, 1119, 1359 (1965); **17**, 1313 (1966).
13) R. K. Ahrenkiel, *J. Opt. Soc. Am.*, **61**, 1651 (1971).
14) Y. Oyanagi, Subprogram POWl, Program Library, Computer Centre, Univ. of Tokyo.
15) T. Ohta, H. Kuroda, T. L. Kunii, *Theor. Chim. Acta (Berl.)*, **19**, 167 (1970).
16) K. Ishii, M. Kinoshita, and H. Kuroda, "Energy and Charge Transfer in Organic Semiconductors," ed by K. Masuda and M. Silver, Plenum Press (1974), p. 177.